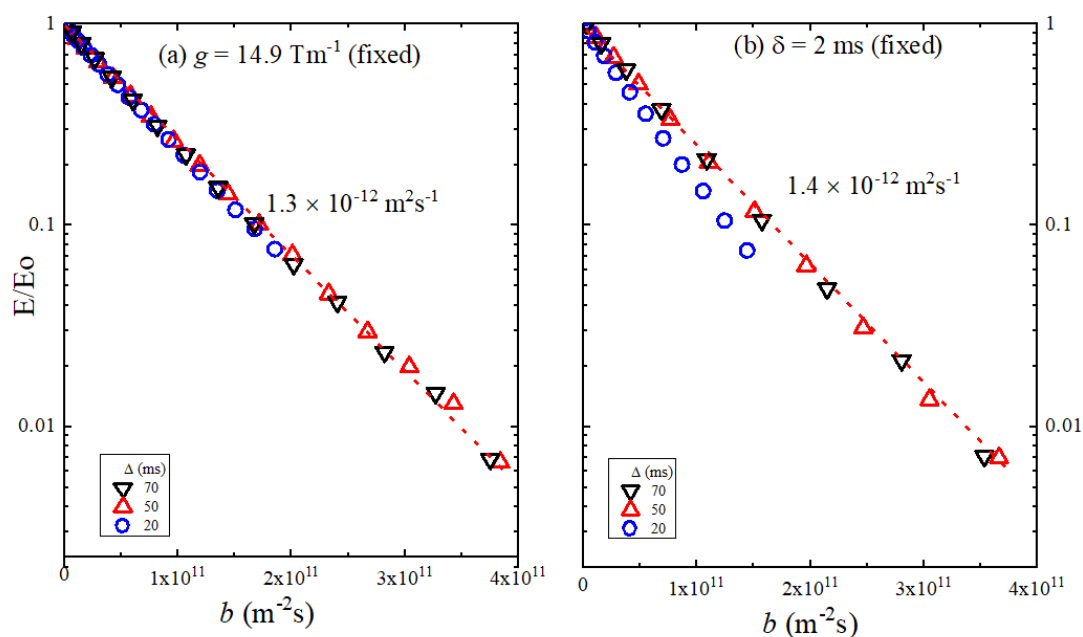


## 1. Stejskal-Tanner Plots for the Li<sup>+</sup> Diffusion in Solution



**Figure S1** Stejskal-Tanner plots for the Li<sup>+</sup> diffusion in viscous polyethylene glycol dimethyl ether (liquid) at 120 °C measured by Hahn echo pulse sequence. (a)  $g$  was fixed at  $14.9 \text{ Tm}^{-1}$  and  $\delta$  varied 0.2 to 4 m for  $\Delta = 20, 50,$  and  $70 \text{ ms}$ , and  $\delta$  was varied 0.2 to 3 ms. (b)  $\delta$  was fixed at 2 ms and  $g$  was varied 1.04 to  $14.9 \text{ Tm}^{-1}$  for  $\Delta = 20, 50,$  and  $70 \text{ ms}$ .

The sample was a liquid polyethylene oxide-based electrolyte doped with  $\text{LiN}(\text{CF}_3\text{SO}_2)_2$  [1]. The Li diffusion in the viscous sample exhibited  $\Delta$ - and  $g$ -dependent phenomena at room temperature. To confirm homogeneous diffusion at the high temperature of 120 °C, the measurements were performed (a) with a fixed  $g$  and varying  $\delta$  and (b) with a fixed and  $\delta$  varying  $g$ . The anomalous diffusion effects appeared slightly in a  $\delta$  fixed  $g$  varied plot at  $\Delta = 20 \text{ ms}$ . Several years later, when the sample was left at room temperature to find out why, the sample had turned into a normal homogeneous liquid.

## 2. Stokes-Einstein Relation of H<sub>2</sub>O

Stokes-Einstein (SE) relation is written as

$$D = \frac{kT}{c \pi \eta r_s} \quad (1)$$

$D$  (diffusion coefficient) and  $\eta$  (viscosity) are experimental data at temperature  $T$ . The  $r_s$  is the Stokes radius of a diffusing molecule (assumed) and  $c$  is a constant between 4 and 6. The SE relation can be rewritten as  $D = \frac{1}{c r_s} \frac{kT}{\pi \eta}$ . Using the reported experimental values of  $D$  and  $\eta$  for H<sub>2</sub>O,  $D$  is plotted versus  $kT/\pi \eta$  in the wide temperature range as shown in Figure S2. From the gradient,  $c r_s$  value can be evaluated.

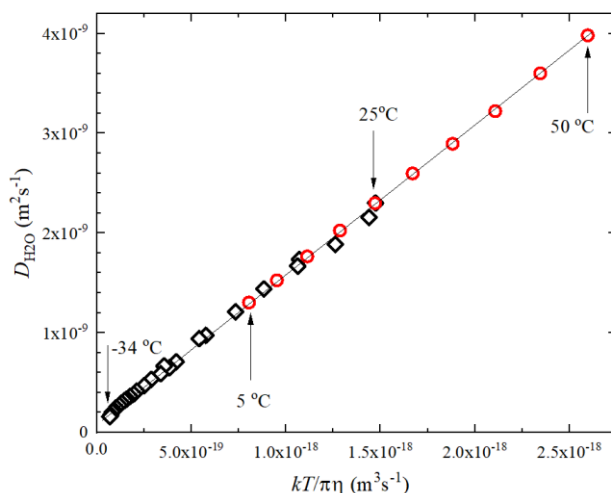


**Figure S2** According to Stokes-Einstein relation, the diffusion coefficient  $D_{\text{H}_2\text{O}}$  is plotted vs  $kT/\pi\eta$  in the temperature range from  $-34$  to  $50^\circ\text{C}$ .  $D$ :  $-34\sim 25^\circ\text{C}$ : Price WS, Ide H, Arata YJ. Phys Chem A. 1999; 103: 448-450. 10.1021/jp9839044.  $D$ :  $5\sim 50^\circ\text{C}$ : Holz M, Heil SR, Sacco A. Phys Chem Chem Phys. 2000; 2: 4740-4742. 10.1039/b005319h.  $\eta$ :  $-34\sim 20^\circ\text{C}$ : Dehaoui A, Issenmann B, Caupin F, 12020–12025, PNAS. 2015; 112. [www.pnas.org/lookup/suppl/doi:10.1073/pnas.1508996112/-/DCSupplemental](http://www.pnas.org/lookup/suppl/doi:10.1073/pnas.1508996112/-/DCSupplemental).  $\eta$ :  $2\sim 50^\circ\text{C}$ : <https://wiki.anton-paar.com/jp-jp/water/>, accessed June 15, 2021.

Experimental gradient,  $cr_s = 671$  pm. A widely accepted  $r_s(\text{H}_3\text{O}^+) = 141$  pm gives  $c = 4.8$ .

### 3. Nernst-Einstein Type Plots of $D_{\text{Li}}-\sigma$ and $N_{\text{NE}}-\sigma$ for Inorganic Solid Electrolytes

The relationship between  $D_{\text{Li}}$  and  $\sigma$  is one of the most important subjects in electrochemistry. Following the Nernst-Einstein (NE), the relations for solid inorganic electrolytes are given as follows [2],

$$D_{\text{Li}}(T) = \frac{kT}{N_{\text{NE}}e^2} \sigma(T), \quad N_{\text{NE}} = \frac{kT\sigma(T)}{e^2 D_{\text{Li}}(T)}. \quad (2)$$

The experimental values of  $D_{\text{Li}}$  were plotted versus  $\sigma$  in Figure S3 (a) and  $N_{\text{NE}}$  calculated from  $D_{\text{Li}}$  and  $\sigma$  values were plotted in Figure S3 (b). The  $D_{\text{Li}}$  were obtained as an equilibrated value at long  $\Delta$  at room temperature including recently published values.

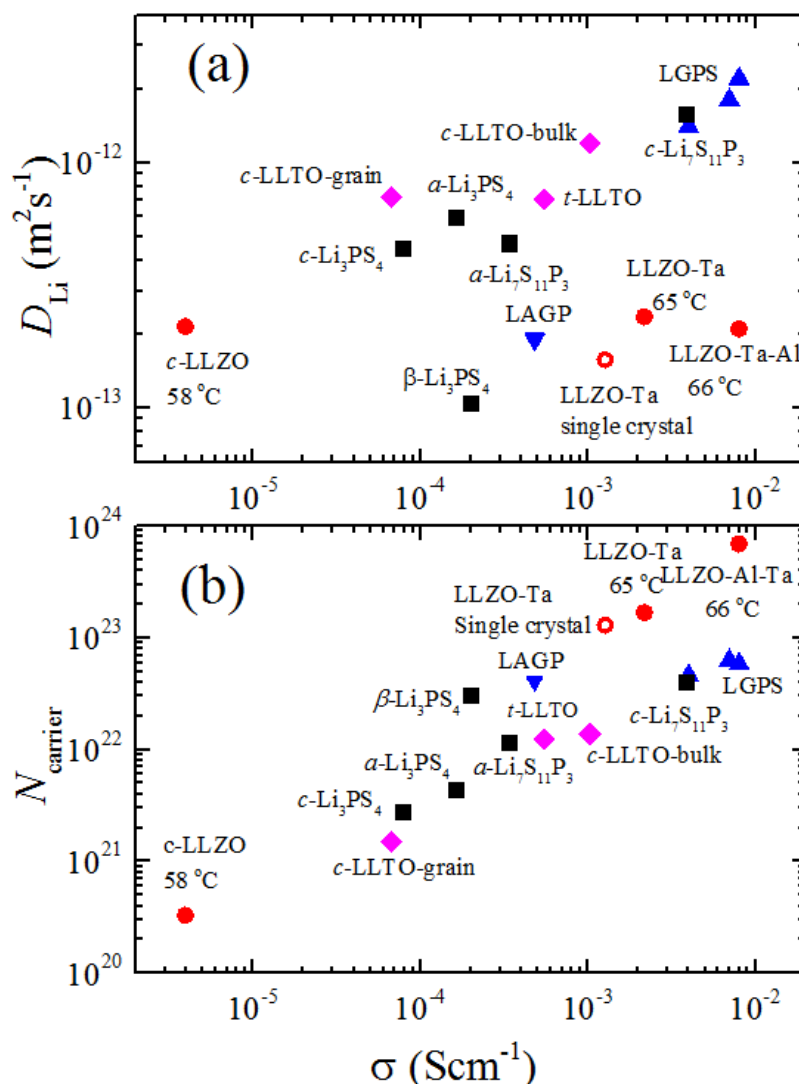


**Figure S3** (a)  $D_{Li}$  versus  $\sigma$  at room temperature except for the garnets for which the temperatures are shown; c-LLZO at 58 °C [3], LLTO [4], LAGP [5], amorphous and crystal Li<sub>3</sub>PS<sub>4</sub> [6],  $\beta$ -Li<sub>3</sub>PS<sub>4</sub> [7], Li<sub>7</sub>S<sub>11</sub>P<sub>3</sub> [8, 9], LGPS [10, 11], LLZO-Ta and LLZO-Al-Ta at elevated temperatures [12] and LLZO-Ta single-crystal [13]. (b) The carrier number,  $N_{carrier}$  estimated by the NE equation plotted versus  $\sigma$ .

A detailed description was given in References [14] and [15].

#### 4. Stack Plots of Real and Magnitude Components for 1 mm Disk Sample of Single Crystal of LLZO-Ta Placed Vertically to the PFG Direction

The Fourier transformed spectra of the echo-attenuation decay are observed in the PFG-NMR measurements following the pulse sequence in Figure 2. The signals consist of real and imaginary components and the magnitude is calculated by  $magnitude = \sqrt{real^2 + imaginary^2}$ . Mostly, similar patterns of real components and the calculated magnitude are observed. When the diffracted patterns are observed, the real component includes negative values.

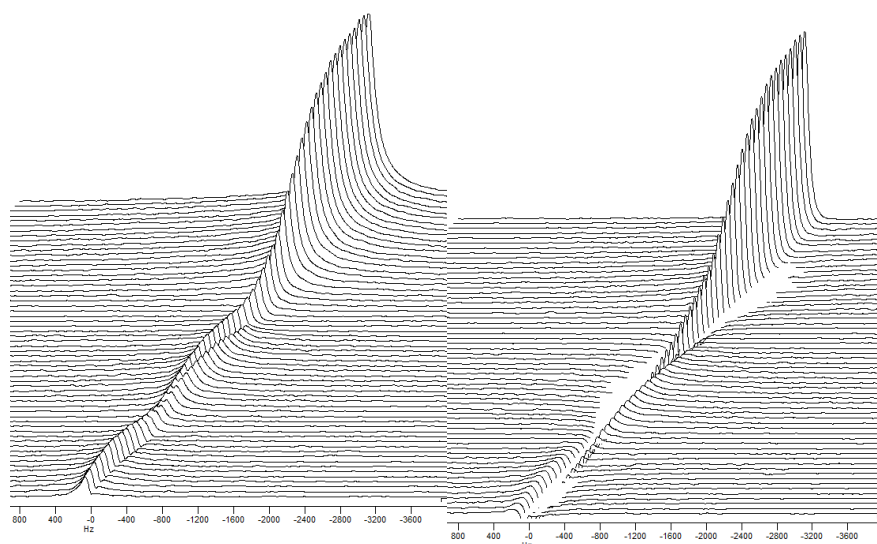


**Figure S4** Stack plots of echo attenuation spectra for the disk sample (1 mm thick, 4 mm diameter) placed vertically to the PFG direction ( $g = 10.0 \text{ Tm}^{-1}$ ), at  $\Delta = 10 \text{ ms}$  with varying  $\delta = 0.2$  to  $8 \text{ ms}$  (60 points) at  $28^\circ\text{C}$ . The signal position was set near  $0 \text{ Hz}$ . The echo attenuation signals were observed from  $\delta = 0.2 \text{ ms}$  (top) to  $\delta = 8 \text{ ms}$  (bottom). Left: magnitude, right: phase sensitive real mode.

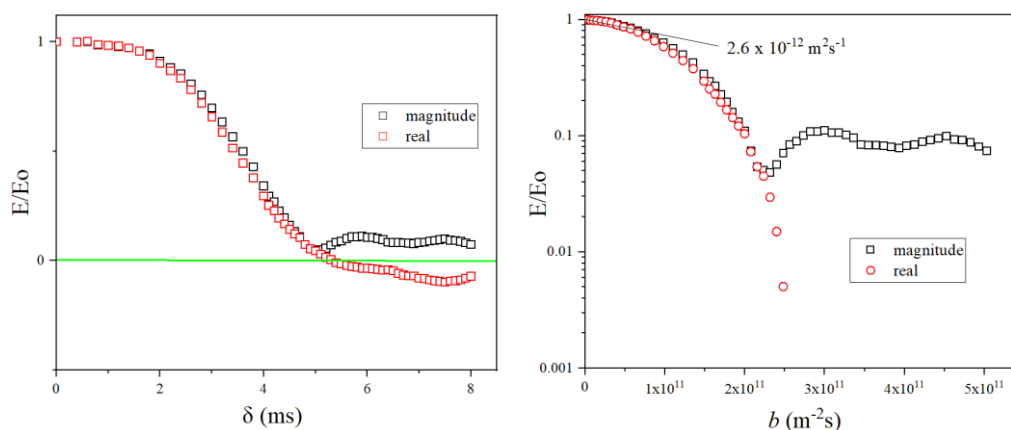


**Figure S5** The normalized intensities of real component and the magnitude are plotted versus  $\delta$  (left) and the Stejskal and Tanner plots vs  $b$  in the *semi-logarithmic* graph (right).

### 5. Stack Plots of Real, Imaginary, and Magnitude Components for the 1 mm Disk Sample of the Single Crystal LLZO-Ta Placed Horizontally to the PFG Direction

Unusually, the real and imaginary components of the echo attenuation decays show sinusoidal patterns. This is the first observation for the thin disk sample of a single crystal of LLZO-Ta placed horizontally to the PFG direction.

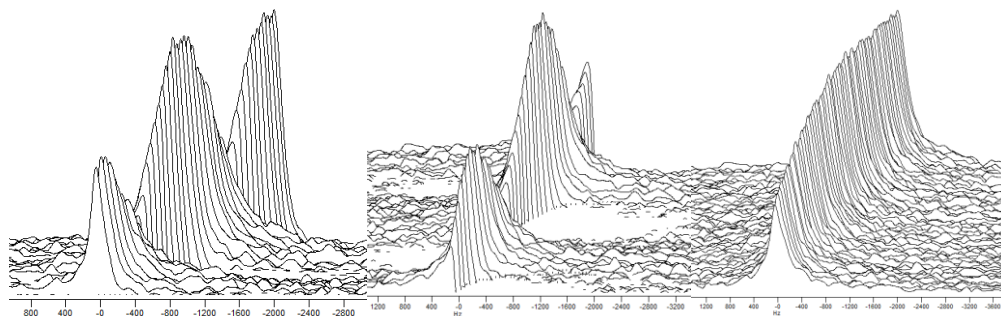


**Figure S6** The stack plot profiles of echo attenuation decays for a 1 mm disk sample placed horizontally to the PFG ( $g = 10.0 \text{ Tm}^{-1}$ ), at  $\Delta = 10 \text{ ms}$  with varying  $\delta = 0.2$  to 8 ms (60 points) at  $28^\circ\text{C}$ . The signal position was set near 0 Hz and the echo signals were observed at  $\delta = 0.2 \text{ ms}$  (top) to  $\delta = 8 \text{ ms}$  (bottom). Left: real mode, middle: imaginary mode, right: magnitude mode. This is the first observation of sinusoidal patterns in the real and imaginary components.

The plots of the three components versus  $\delta$  are shown in Figure 9.

## References

- Hayamizu K, Sugimoto K, Akiba E, Aihara Y, Bando T, Price WS. An NMR and ionic conductivity study of ion dynamics in liquid polyethylene oxide-based electrolytes doped with  $\text{LiN}(\text{CF}_3\text{SO}_2)_2$ . *J Phys Chem B* 2002; 106; 547-554.
- Julien C, Nazri GA. Solid state batteries: Material design and optimization. Boston: Kluwer Academic Publishers; 1994.
- Hayamizu K, Seki S, Haishi T. Lithium ion micrometer diffusion in a garnet-type cubic  $\text{Li}_7\text{La}_3\text{Zr}_2\text{O}_{12}$  (LLZO) studied using  $^7\text{Li}$  NMR spectroscopy. *J Chem Phys.* 2017; 146: 024701.
- Hayamizu K, Seki S, Haishi T.  $^7\text{Li}$  NMR diffusion studies in micrometre-space for perovskite-type  $\text{Li}_{0.33}\text{La}_{0.55}\text{TiO}_3$  (LLTO) influenced by grain boundaries. *Solid State Ion.* 2018; 326: 37-47.
- Hayamizu K, Seki S. Long-range Li ion diffusion in NASICON-type  $\text{Li}_{1.5}\text{Al}_{0.5}\text{Ge}_{1.5}(\text{PO}_4)_3$  (LAGP) studied by  $^7\text{Li}$  pulsed-gradient spin-echo NMR. *Phys Chem Chem Phys.* 2017; 19: 23483-23491.
- Hayamizu K, Aihara Y, Watanabe T, Yamada T, Ito S, Machida N. NMR studies on lithium ion migration in sulfide-based conductors, amorphous and crystalline  $\text{Li}_3\text{PS}_4$ . *Solid State Ion.* 2016; 285: 51-58.
- Stöffler H, Zinkevich T, Yavuz M, Senyshyn A, Kulisch J, Hartmann P, et al.  $\text{Li}^+$  ion dynamics in  $\beta$ - $\text{Li}_3\text{PS}_4$  observed by NMR: Local hopping and long-range transport. *J Phys Chem C.* 2018; 122: 15954-15965.
- Hayamizu K, Aihara Y. Lithium ion diffusion in solid electrolyte  $(\text{Li}_2\text{S})_7(\text{P}_2\text{S}_5)_3$  measured by pulsed-gradient spin-echo  $^7\text{Li}$  NMR spectroscopy. *Solid State Ion.* 2013; 238: 7-14.
- Hayamizu K, Aihara Y, Machida N. Anomalous lithium ion migration in the solid electrolyte  $(\text{Li}_2\text{S})_7(\text{P}_2\text{S}_5)_3$ ; fast ion transfer at short time intervals studied by PGSE NMR spectroscopy. *Solid State Ion.* 2014; 259: 59-64.
- Kuhn A, Duppel V, Lotsch BV. Tetragonal  $\text{Li}_{10}\text{GeP}_2\text{S}_{12}$  and  $\text{Li}_7\text{GePS}_8$ -exploring the Li ion dynamics in LGPS Li electrolytes. *Energy Environ Sci.* 2013; 6: 3548-3552.
- Kuhn A, Gerbig O, Zhu C, Falkenberg F, Maier J, Lotsch BV. A new ultrafast superionic Li-

- conductor: Ion dynamics in  $\text{Li}_{11}\text{Si}_2\text{PS}_{12}$  and comparison with other tetragonal LGPS-type electrolytes. *Phys Chem Chem Phys*. 2014; 16: 14669-14674.
12. Matsuda Y, Itami Y, Hayamizu K, Ishigaki T, Matsui M, Takeda Y, et al. Phase relation, structure and ionic conductivity of  $\text{Li}_{7-x-3y}\text{Al}_y\text{La}_3\text{Zr}_{2-x}\text{Ta}_x\text{O}_{12}$ . *RSC Adv*. 2016; 6: 78210-78218.
  13. Kataoka K, Akimoto J. High ionic conductor member of garnet-type oxide  $\text{Li}_{6.5}\text{La}_3\text{Zr}_{1.5}\text{Ta}_{0.5}\text{O}_{12}$ . *ChemElectroChem*. 2018; 5: 2551-2557.
  14. Hayamizu K.  $^7\text{Li}$  spin echo NMR diffusion studies. *Annu Rep NMR Spectrosc*. 2019; 98: 57-123.
  15. Hayamizu K, Terada Y, Kataoka K, Akimoto J, Haishi T. Relationship between  $\text{Li}^+$  diffusion and ion conduction for single-crystal and powder garnet-type electrolytes studied by  $^7\text{Li}$  PGSE NMR spectroscopy. *Phys Chem Chem Phys*. 2019; 21: 23589-23597.